Available online at www.sciencedirect.com
ScienceDirect
Trans. Nonferrous Met. Soc. China 21(2011) 2348−2357
Transactions of Nonferrous Metals Society of China
www.tnmsc.cn

Hot corrosion behavior of Ni−*x*Cr−6.8Al based alloys

HAN Chao[1], LIU Yong[1], WANG Yan[1], LI Wei-jie[1], TANG Hui-ping[2]

1. State Key Laboratory of Powder Metallurgy, Central South University, Changsha 410083, China;
2. State Key Laboratory of Porous Metals Materials, Northwest Institute for Nonferrous Metal Research, Xi'an 710016, China

Received 1 March 2011; accepted 6 September 2011

Abstract: The hot corrosion behaviors of as-cast and preoxidized Ni−*x*Cr−6.8Al based alloys in the mixture of Na_2SO_4+25%NaCl at 873 K were studied. The results show that the mass loss of Ni−*x*Cr−6.8Al based alloys decreases with the increase of Cr content. Preoxidation improves the resistance to corrosion regardless of the concentration of Cr. The kinetics of as-cast Ni−12Cr−6.8Al and Ni−16Cr−6.8Al based alloys fits the parabolic law well, while that of the as-cast Ni−20Cr−6.8Al based alloy fits the power law. The kinetics of all the preoxidized samples obey the logarithmic law. The mechanism of the as-cast alloys can be well explained by the acid-base melting model. The behavior of the preoxidized alloys is found to be mainly determined by the properties of the oxide layer formed during the preoxidation to a large extend.

Key words: Ni-Cr-Al based alloy; hot corrosion; Cr content; preoxidation; kinetics; corrosion mechanism

1 Introduction

Ni−Cr−Al based alloy is a widely used superalloy which offers an attractive combination of superior mechanical strength at high temperatures with good resistance to oxidation. It is mainly applied to the aviation and navigation gas-turbine engine as well as the coal-combustion gas filter, the service conditions of which are very complex. Besides oxidation, there are some depositions on the work piece such as sulfate, halide and other sulphonates. A much heavier corrosion oxidation would then occur, which is called hot corrosion [1].

Although lots of works have been done on hot corrosion, much attention has been paid to binary alloys such as Ni−Al, Ni−Cr, Fe−Al. NIU et al [2] studied the hot corrosion behavior of Ni−Al intermetallic compound in the combustion gas at 600−800 °C and proved that the appearance of sulfides accelerated the hot corrosion. They also found that the hot corrosion of Ni−Al intermetallic compound was involved in a variable different corrosion mechanisms, including scale fluxing which concerned mostly Ni oxide at 873 K, mixed oxidation-sulfidation and scale fluxing mechanism at 973 and 1 073 K. OU et al [3] showed that the kinetics of Ni−Cr coatings which were corroded with a molten K_2SO_3+25% Na_2SO_3 salt layer at 923 K followed the parabolic law, and classic fluxing model was used to explain the mechanism. Concerning the mechanism of hot corrosion, GLOBEL and PETTIT [4] and BORNSTEIN and De CRESCENTE [5] showed the formation of sulfide indeed resulted from the reaction of the metallic substrate with a thin film of fused salt, and an acid-base melting model was proposed [7−10]. RAPP [11] further consummated their model. Other mechanisms of hot corrosion include the electrochemistry model and oxidation-sulfidation model, etc. So far, limited information is available on the hot corrosion behavior of ternary Ni−Cr−Al alloy, especially at temperature below the melting point of the salts, which is usually called low temperature hot corrosion (LTHC).

This study focused on the relationship between the concentration of Cr, preoxidation and the LTHC behavior of Ni−Cr−Al based alloy. The mechanisms of LTHC for Ni−Cr−Al alloy with different initial states were also discussed.

Foundation item: Project (2009AA032601) supported by the National High-tech Research and Development Program of China; Project supported by the Postdoctoral Science Foundation of Central South University, China
Corresponding author: WANG Yan; Tel: +86-731-88877495; Fax: +86-731-88877132; E-mail: wangyan@mail.csu.edu.cn
DOI: 10.1016/S1003-6326(11)61019-4

2 Experimental

The compositions of the Ni−Cr−Al based alloys are listed in Table 1. In the text below, the alloys were simply called Ni−12Cr−6.8Al, Ni−16Cr−6.8Al and Ni−20Cr−6.8Al alloys, respectively. The alloys were cut into samples with size of 10 mm×10 mm×4 mm from the original ingots obtained by 3−4 times arc melting of pure metal in argon. Then, the samples were polished through No.1000 carborundum paper before being washed in alcohol and acetone. The preoxidation treatment was carried out in a horizontal tube furnace with three heating zones at 1 273 K for 50 h with the nitrogen flow rate of 0.03 m^3/h.

Table 1 Compositions of tested alloys (mass fraction, %)

Alloy	Cr	Al	Fe	Mn	Si
Ni−12Cr−6.8 Al	12	6.8	3	0.05	0.2
Ni−16Cr−6.8 Al	16	6.8	3	0.05	0.2
Ni−20Cr−6.8 Al	20	6.8	3	0.05	0.2
Alloy	Y	B	Zr	C	Ni
Ni−12Cr−6.8 Al	0.01	0.01	0.1	0.05	Bal.
Ni−16Cr−6.8 Al	0.01	0.01	0.1	0.05	Bal.
Ni−20Cr−6.8 Al	0.01	0.01	0.1	0.05	Bal.

After being immersed into a mixture of 75% Na_2SO_4+25% NaCl (mass fraction), the as-cast and preoxidized samples were put into the furnace which was already heated to 873 K. The samples were taken out every 25 h and the corrosion products on the surface were removed. The mass loss was measured by an electrobalance with an accuracy of 0.1 μg.

Both the samples before and after LTHC were examined by means of X-ray diffraction (XRD) and scanning electron microscopy (SEM) equipped with an energy-dispersive X-ray microanalysis (EDX) in order to establish the compositions of the scales and the spatial distributions of the elements as well as the phases.

3 Results

3.1 Hot corrosion kinetics

The kinetics curves of the samples corroded in the sodium sulfate+sodium chloride salt at 873 K are shown in Fig. 1. Most of the curves exhibit the same tendency except the Ni−12Cr−6.8Al and Ni−16Cr−6.8Al alloys, since their curves reach much higher with corrosion time increasing. The mass loss of Ni−12Cr−6.8Al alloy after heating for 25 h even reaches 37.54 mg/cm^2, while that for Ni−16Cr−6.8Al alloy reaches 6.23 mg/cm^2, and that for Ni−20Cr−6.8Al alloy reaches 3.42 mg/cm^2, respectively. This indicates that Ni−12Cr−6.8Al alloy undergoes a catastrophic corrosion. The mass loss of Ni−20Cr−6.8Al alloy maintains around 6 mg/cm^2 after 50 h, which is even lower than that of the preoxidized Ni−12Cr−6.8Al alloy (Fig. 1). Therefore, it can be concluded that with the increase of the Cr content, the mass loss of the alloy decreases. In other words, Cr improves the resistance to hot corrosion of the Ni−Cr−Al based alloys. Interestingly, the mass loss of the preoxidized samples shows much less dependence on the Cr content (Fig. 1(c)). With the increase of Cr, the mass loss maintains 7.0, 1.75 and 4.87 mg/cm^2 after 25 h, respectively. It is suggested that there are different mechanisms operated in the as-cast and preoxidized alloys. Compared with the as-cast alloys, the mass loss of preoxidized samples is much less, which indicates that

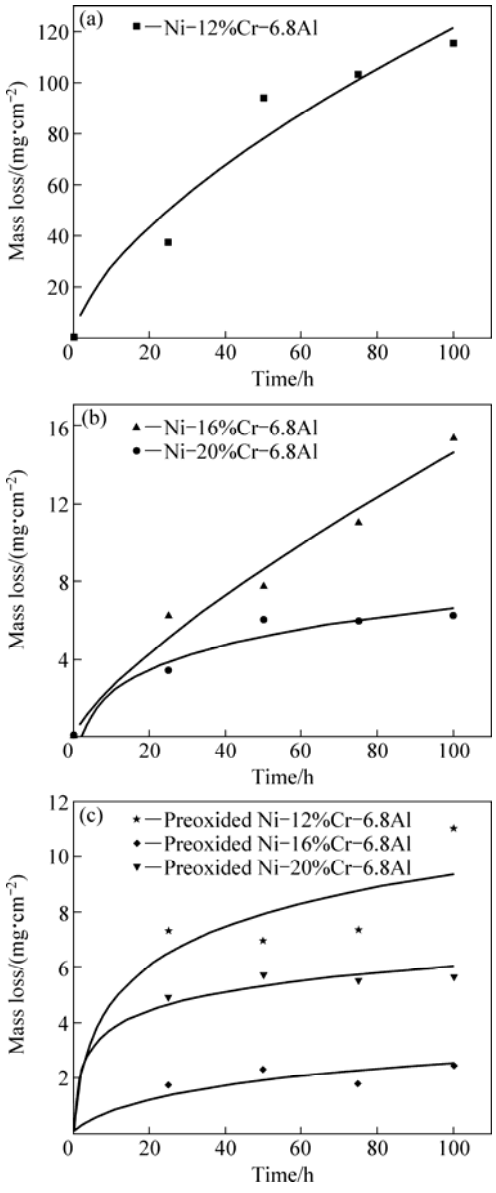

Fig. 1 Kinetics curves for Ni−*x*Cr−6.8Al based alloys corroded in sodium sulfate+25% sodium chloride salt at 873 K: (a) Ni−12Cr−6.8Al alloy; (b) Ni−16Cr−6.8Al and Ni−20Cr−6.8Al alloys; (c) Preoxidized alloys

the preoxidation is effective to protect the tested alloys from hot corrosion (Fig. 1).

3.2 Microstructures of Ni−Cr−Al based alloys before hot corrosion

Figure 2 shows the XRD patterns of the as-cast and preoxidized alloys before hot corrosion. All the as-cast samples are composed of γ phase (solid solution) and γ' phase (Ni_3Al), as shown in Fig. 2(a). After preoxidation, an oxide layer composed of mainly alumina with minor chromia and spinel is generated on the surface of the as-cast alloy (Fig. 2(b)). This is in agreement with the theory by FELIX [12] that if the mass ratio of Cr to Al is less than 4, the alloy would be mainly covered by alumina layer. From the microstructure of the oxide layer in Fig. 3, it can be seen that although the chemical compositions of oxide layer are almost the same, there are still some obvious differences (see Table 2). Preoxidized Ni−16Cr−6.8Al alloy has the thickest oxide layer which is not easy to spall (Fig. 3(b)), while preoxidized Ni-20Cr-6.8Al has the least protective oxide layer (Fig. 3(c)).

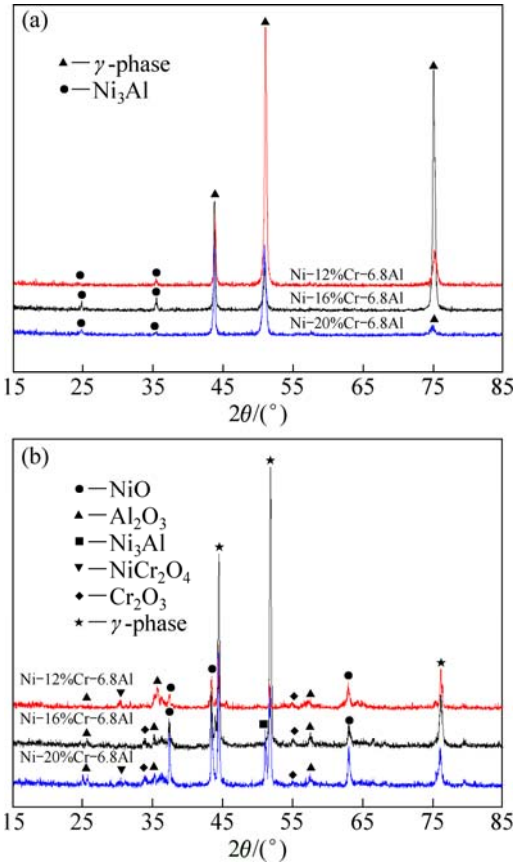

Fig. 2 XRD patterns of Ni−*x*Cr−Al alloys before hot corrosion: (a) As-cast samples; (b) Preoxidized samples

3.3 Microstructures of Ni−Cr−Al based alloys after hot corrosion

Figure 4(a) reveals the catastrophic corrosion occurring on the as-cast Ni−12Cr−6.8Al alloy. The thickness of the corrosion layer which is mainly made up of bitty oxides and salts reaches 800 μm. Figure 4(b) shows the SEM image at high magnification of region *A* in Fig. 4(a). Table 3 lists the compositions at different

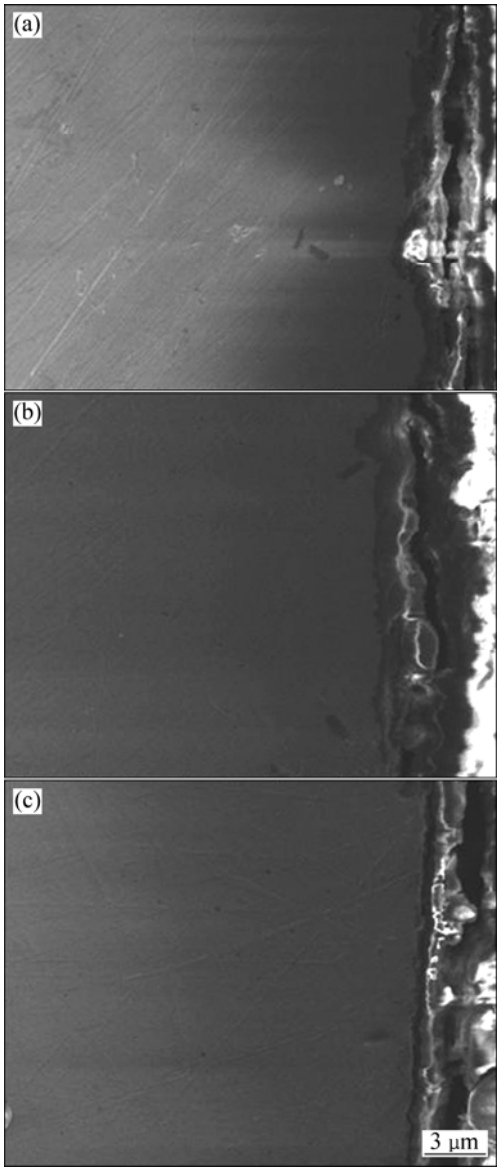

Fig. 3 SEM images of cross-section for preoxidized samples before hot corrosion: (a) Ni−12Cr−6.8Al; (b) Ni−16Cr−6.8Al; (c) Ni−20Cr−6.8Al

Table 2 Comparison of oxide layers formed on preoxidized Ni−*x*Cr−Al based alloys

Sample	Composition	Thickness/μm	Adhesion
Ni−12Cr−6.8 Al	Al_2O_3, Cr_2O_3, $NiCr_2O_4$	1.5	Good
Ni−16Cr−6.8 Al	Al_2O_3, Cr_2O_3, $NiCr_2O_4$, $NiAl_2O_4$	2.8	Good
Ni−20Cr−6.8 Al	Al_2O_3, Cr_2O_3	1.0	Bad

position in Fig. 4(b). Composition of position *B* which is on the left side of the crack in region *A* is mainly made up of compact oxides of Al and Cr, while on the right side, the composition of position *C* is nearly the same with that of the substrate. The compositions of positions *D* and *E* near the crack consist of sulfides of Ni and oxides of Ni, respectively. It should be noted that the salts are not only padded in the crack, but also penetrated in the oxide layer and formed particles in different shapes. Figure 4(c) shows the mud-like Ni oxide precipitation and pitting of the alloy generated during the hot corrosion. The NiO is loose and it is easy to spall from the substrate (Fig. 4(c)). The pitting corrosion can be regarded as a universal phenomenon in LTHC of alloys.

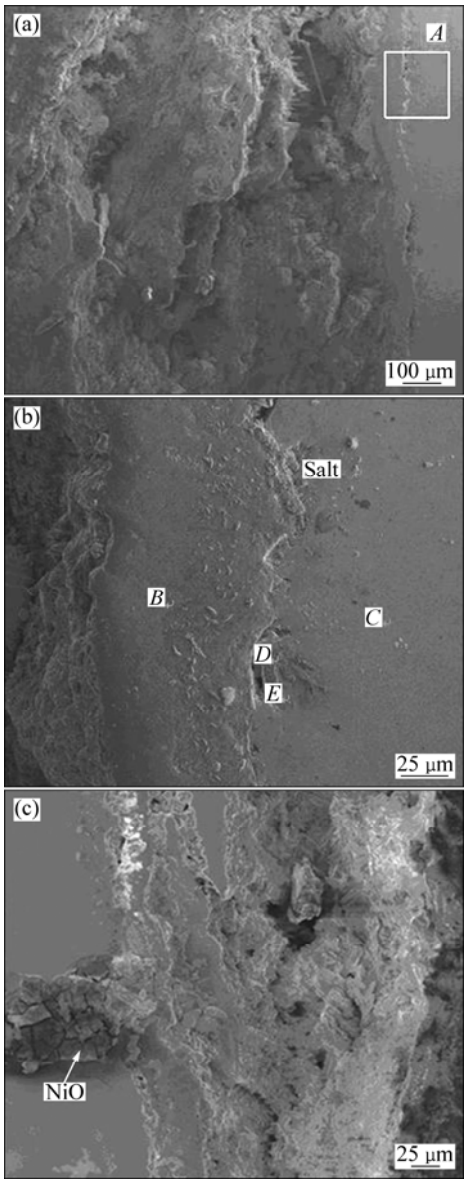

Fig. 4 SEM images of cross-section for Ni−12Cr−6.8Al alloy after hot corrosion at 873 K for 100 h: (a) Low magnification; (b) High magnification of region *A* in Fig. 4(a); (c) NiO precipitation and pitting

Table 3 Composition analysis of alloy in Fig. 4(b) (mass fraction, %)

Position	Composition/%					
	Ni	Cr	Al	S	O	Fe
B	8.00	21.79	22.06	2.31	44.22	1.63
C	71.68	12.41	9.23	0	2.72	3.95
D	56.23	1.72	1.28	24.42	15.79	0.56
E	65.08	4.32	10.21	0.46	18.41	1.51

Compared with Ni−12Cr−6.8Al alloy, much less corrosion occurs in the Ni−16Cr−6.8Al alloy, with only a 10 μm thick corrosion layer and corrosion affected zone at the top left corner of the substrate (Fig. 5). The corrosion layer contains some oxides such as Al_2O_3, Cr_2O_3, NiO and sulfides of Ni and Cr. The hot corrosion affected zone with the maximum depth of 20 μm contains less Al and Cr than the substrate, and almost contains no S. Meanwhile, there is a clear crack between the corrosion layer and the substrate, as seen from Fig. 5(a).

There are only a few scattered corrosion layers which are made up of oxides of Al, Cr and sulfides. Most of the surface is covered by a compact thin layer of oxides with the thickness of 1−2 μm and the main compositions are oxides of Cr and Al. No obviously affected zone is observed in the cross-section of the as-cast Ni−20Cr−6.8 Al alloy. From the kinetics, the Ni−20Cr−6.8Al alloy suffers less hot corrosion among the as-cast alloys. The results obtained from Fig. 6 fit well with the above results.

Figure 7 shows the XRD patterns of the as-cast alloys after LTHC. It can be seen that after hot corrosion at 873 K for 100 h in the mixtures, the XRD pattern of Ni−12Cr−6.8Al alloy displays a strong peak of NiO which is even higher than that of the substrate. In addition, there are also obvious peaks of Ni_3S_2 and a little spinel of Cr. Other peaks of Ni−12Cr−6.8Al alloy refer to sodium chloride and sodium sulfate. Ni−16Cr−6.8Al alloy only has peaks of Ni oxide, while Ni−20Cr−6.8Al alloy has both chromia and NiO peaks. The result of XRD is in conformity with the SEM observations and EDX analysis.

Figure 8 shows the SEM images of the preoxidized Ni−12Cr−6.8Al alloy after hot corrosion at 873 K for 100 h. Table 4 shows the results of EDX analysis of different positions in Fig. 8(b).

Although the resistance to hot corrosion of the alloy is remarkably improved due to the oxide layer, the poor binding force makes it easy to spall from the substrate after hot corrosion. After spalling of the corrosion layer, internal oxidation in the substrate occurs, as shown in Fig. 8(b). The thickness of internal oxidation zone is about 100 μm, and the composition is poor in Cr and Al but rich in Ni and O. At the region about 50 μm from the

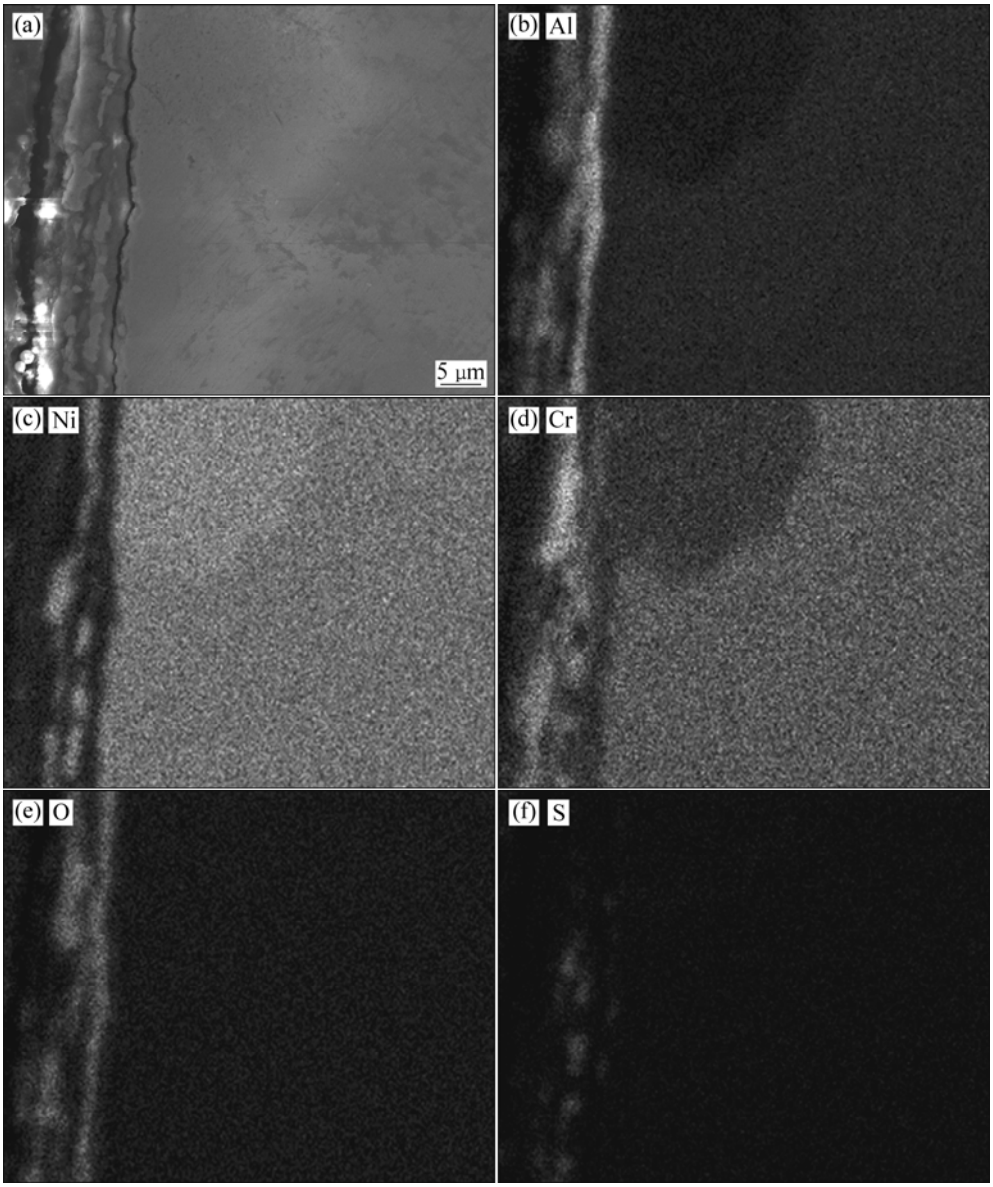

Fig. 5 SEM images (a) of cross-section for Ni−16Cr−6.8Al alloy after hot corrosion at 873 K for 100 h and distribution of Al (b), Ni (c), Cr (d), O (e), S (f)

surface, the shape of the oxides is chock-like (Fig. 8(b), position *B*), while the oxides become tiny with increasing distance (Fig. 8(b), position *C*). In addition, the content of sulfur in positions *B* and *C* is more or less the same with that in Table 4.

The corroded layer of preoxidized Ni−16Cr−6.8Al alloy after hot corrosion at 873 K for 100 h is about 10 μm (Fig. 9). The composition of the corroded layer is almost the same with that of the as-cast alloy, which mainly contains the oxides of Ni, Al, Cr and S. The maximum depth of the affected zone is around 15 μm.

In comparison with Fig. 9, the corrosion layer of preoxidized Ni−20Cr−6.8Al alloy is much thinner and is not well-distributed along the direction of thickness (Fig. 10(a)), although the compositions are almost the same (Fig. 10(b)). The corrosion layer of preoxided Ni−20Cr−6.8Al sticks to the substrate closely, beneath which there is an obviously affected zone with mean thickness of around 15 μm. The layer marked by the arrow in Fig. 10(a) is determined to be the sulfides of Cr and Ni.

Figure 11 shows the XRD patterns of the preoxidized samples after hot corrosion at 873 K for 100 h. Compared with the corroded samples of the as-cast alloy, the corrosion products mainly consist of oxide scales such as alumina, chromia and NiO, and no sulfides are detected. It may also be noted that after hot corrosion, the diffraction patterns of the corroded samples for

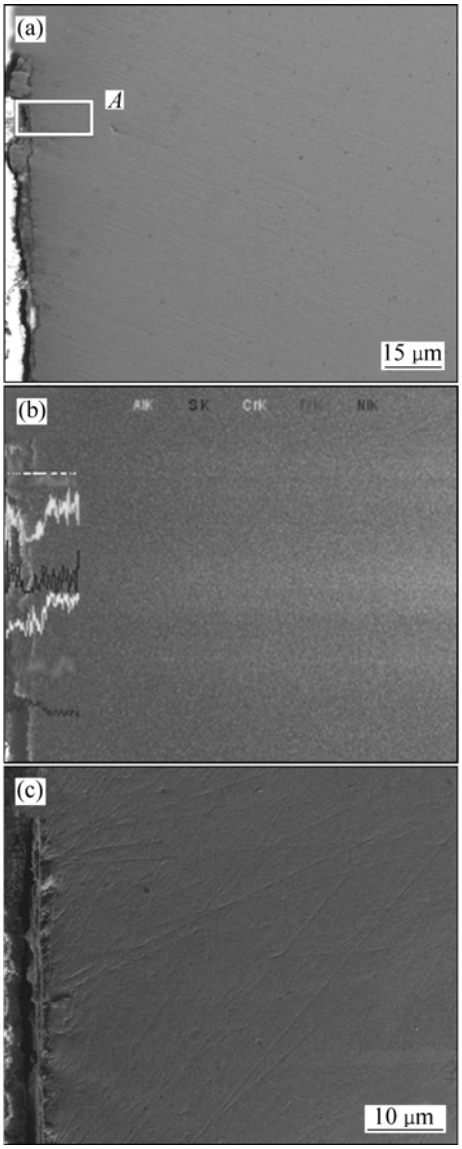

Fig. 6 SEM images of cross-section for Ni−20Cr−6.8Al alloy after hot corrosion at 873 K for 100 h: (a) Low magnification; (b) Line scanning analysis; (c) High magnification of region *A*

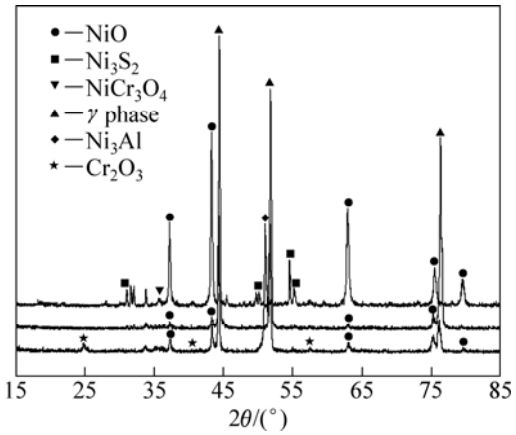

Fig. 7 XRD patterns of as-cast alloys after hot corrosion at 873 K for 100 h

preoxidized alloys show remarkably higher peaks of NiO compared with those of the corresponding samples before hot corrosion. The results are quite consistent with the SEM images and EDX analysis.

4 Discussion

The appearance of a molten salt layer is known to be a fundamental prerequisite for the occurrence of hot corrosion [2]. Although the melting point of sodium chloride is 1 071 K and the eutectic melting point for sodium chloride and sodium sulfate is about 898 K. NIU et al [2] demonstrated that the Ni−Al intermetallic compound underwent a hot corrosion attack even with deposits of pure sodium sulfate at 873 K. The formation of a liquid solution of metal sulfates involving both Ni and Al is thought to be the probable reason that the hot

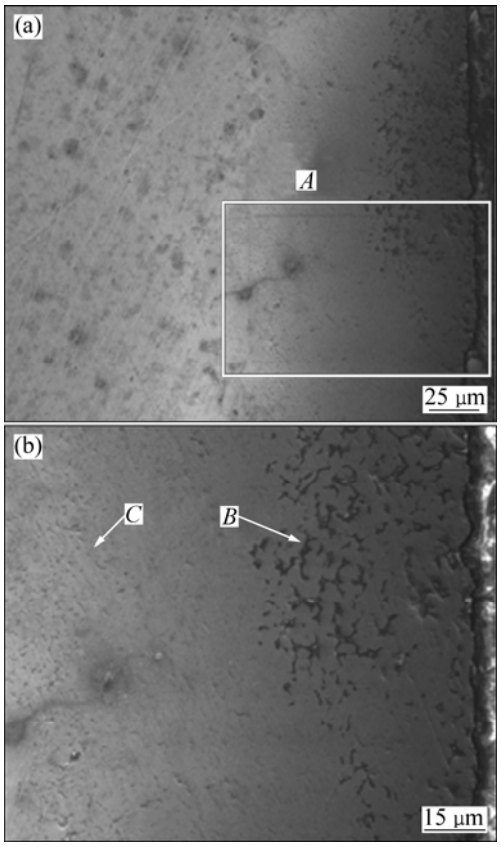

Fig. 8 SEM images of cross-section of preoxidized Ni−12Cr−6.8 Al alloy after hot corrosion at 873 K for 100 h: (a) Low magnification; (b) High magnification of region *A*

Table 4 Composition analysis of alloy at different positions in Fig. 8(b) (mass fraction)

Position	Composition/%				
	Ni	Cr	Al	S	O
B	88.40	0.70	0.68	8.32	0.15
C	74.32	2.97	0.55	20.12	0.17

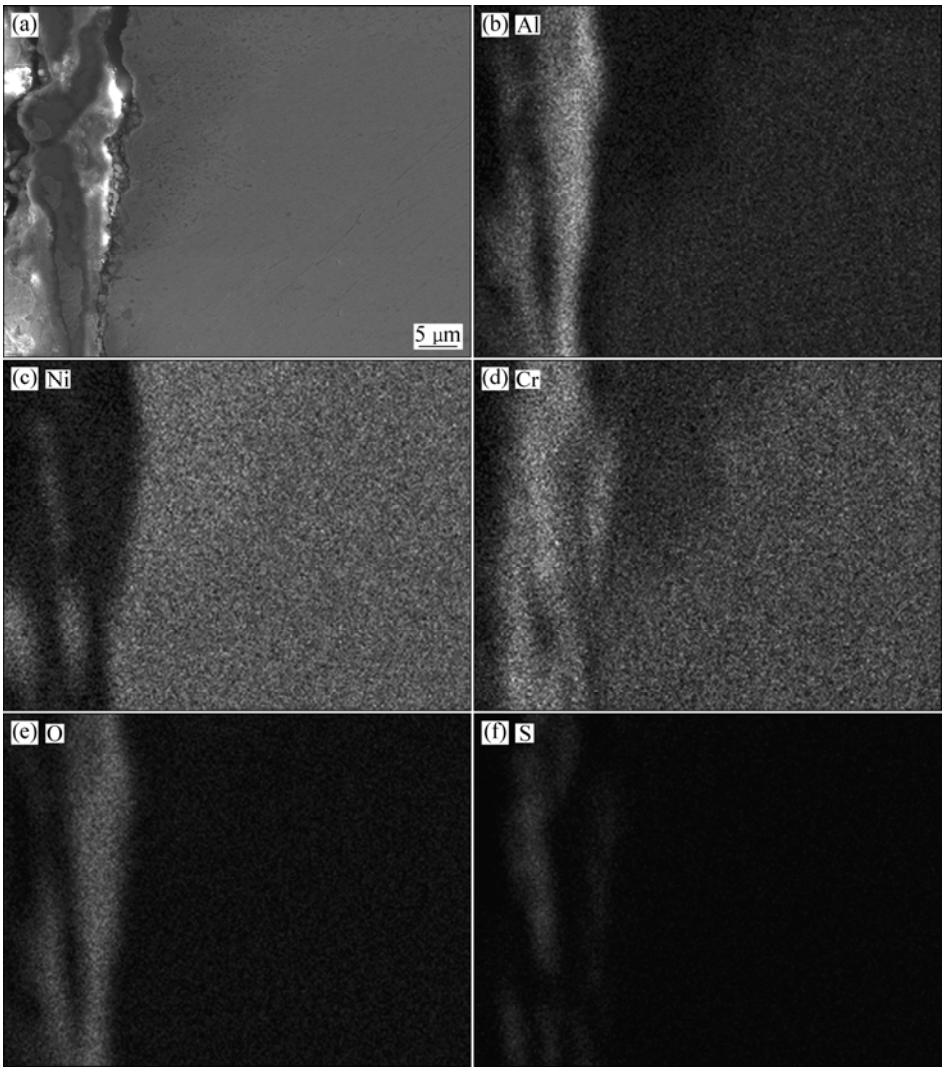

Fig. 9 SEM images (a) and distribution of Al (b), Ni (c), Cr (d), O (e), S (f) of cross-section for preoxidized Ni−16Cr−6.8 Al after hot corrosion at 873 K for 100 h

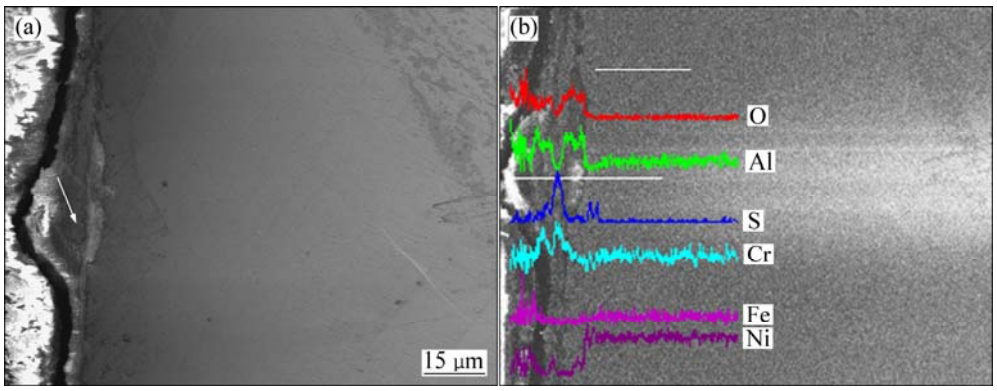

Fig. 10 SEM image (a) and line scanning result (b) of cross-section for preoxidized Ni−20Cr−6.8Al alloy after hot corrosion at 873 K for 100 h

corrosion occurs, since the eutectic point of the solution must be lower than 873 K. As seen in Fig. 4(b), the mixed salt (Na_2SO_4+NaCl) not only distributes in the crack, but also penetrates in the oxide layer to form particles with different shapes. Therefore, it can be determined that LTHC occurs in the salt layer of the tested Ni−Cr−Al based alloys.

From the kinetics curves shown in Fig. 1, the

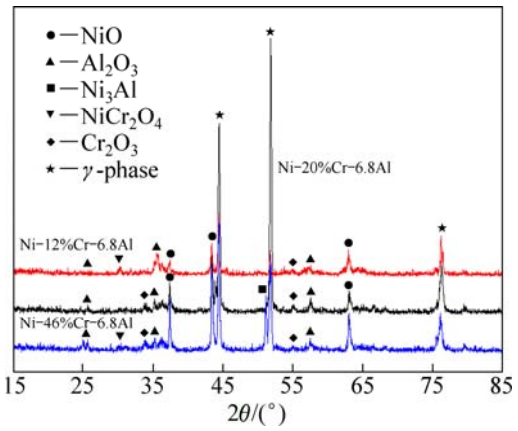

Fig. 11 XRD patterns of preoxidized alloys after hot corrosion at 873 K for 100 h

regression equations are obtained, as listed in Table 5. It is found that the kinetics curves of the alloys all fit the equation $Y=aX^b$ well. Take the existence of initial stage and the error component into consideration, the Ni−12Cr−6.8Al and Ni−16Cr−6.8Al based alloys all fit the parabolic law (b approaches 0.5), while Ni−20Cr−6.8Al based alloy apparently shows a different regime. All the kinetics curves of the preoxidized samples fit the logarithmic law (Table 5). So, the hot corrosion mechanisms operated in the as-cast and preoxidized alloys are quite different.

Table 5 Regression equations of alloys

Alloy	Regression equation	Probability
Ni−12Cr−6.8 Al	$Y=6.51X^{0.63}$	0.92
Ni−16Cr−6.8 Al	$Y=0.45X^{0.75}$	0.93
Ni−20Cr−6.8 Al	$Y=11.86X^{0.11}-12.96$	0.90
Preoxidized Ni−12Cr−6.8 Al	$Y=2.13\ln(X+1.25)-0.46$	0.91
Preoxidized Ni−16Cr−6.8 Al	$Y=\ln(0.12X+1.09)$	0.92
Preoxidized Ni−20Cr−6.8 Al	$Y=\ln(4.14X+1.00)$	0.98

Y presents mass loss (mg/cm^2) and X presents corrosion time (h)

4.1 LTHC mechanism of as-cast Ni−Cr−Al based alloy

As explained by RAPP's model [11], the parabolic law implies that the corrosion is controlled by diffusion and a protective layer may be formed during the process. The following reactions exist in the molten salt layer:

$$SO_4^{2-} \longrightarrow SO_3 + O^{2-} \quad (1)$$

$$SO_3 \longrightarrow 1/2S_2 + 3/2O_2 \quad (2)$$

When the as-cast Ni−Cr−Al alloy contacts with the molten salt, Al_2O_3, Cr_2O_3 and NiO are formed at the interface of alloy and the molten salt, respectively, and lots of oxygen are consumed in the process. According to reaction (2), the pressure of sulfur increases, leading to the formation of sulfides at the interface of oxides and molten salt. Although the stability order of sulfides for Cr, Ni and Al is Cr>Ni>Al, there are mainly sulfides of Ni formed in this investigation as described above. The main reason is that the formation enthalpies of Al_2O_3 and Cr_2O_3 are higher than that of the corresponding sulfides, and the concentration of Ni is much higher than that of Cr. The formation of Ni_3S_2 provides a shortcut to the diffusion of S [2] due to the generation of lots of defects, resulting in the acceleration of hot corrosion. Meanwhile, the composition and distribution of elements in the substrate are changed due to the formation of sulfides, which is apt to oxidation. On the other hand, Ni_3S_2 is easy to react with oxygen, and the reaction between oxygen and sulfides is listed as [13]:

$$2Ni_3S_2 + 7O_2 \longrightarrow 6NiO + 4SO_2 \quad (3)$$

The newly-generated sulfur dioxide can easily diffuse into the deeper substrate and generate new sulfides again. At the same time, because of the consumption of O and S, more oxygen ions are produced at the oxide/salt interface according to reaction (1). The solubility curves of different oxides at 1 200 K and 10^5 Pa oxygen in the fused sodium sulfate developed by RAPP [14] clearly show that NiO, Al_2O_3 and Cr_2O_3 would experience a minimum solubility with the increase of oxygen ions. The basicity dissolution of oxides then begins as:

$$Cr_2O_3 + O^{2-} \longrightarrow 2CrO_2^- \quad (4)$$

$$Al_2O_3 + O^{2-} \longrightarrow 2AlO_2^- \quad (5)$$

Thus the ions formed by reactions (4) and (5) (CrO_2^- and AlO_2^-) would flow outwards to the salt/gas interface where a lower concentration of oxygen ions exists because of exposure into the air. Then the solubility of the oxides decreases and a new incompact layer made up of oxides of Cr and Al forms at the salt/gas interface. As time goes on, the concentration of oxygen ions in the two interfaces tends to the same level. In other words, the molten salt reaches saturation, and the protective oxides layer is stabilized, as shown in Fig. 4(b).

With increasing oxygen ions content, the way of NiO dissolving would shift from the acidity way (in the form of Ni ion) to the basicity way [14]. When Ni oxide is dissolved in the acidity way, the negative gradient of solubility forms. Ni oxide would be continuously dissolved and the catastrophic hot corrosion then occurs. When the salt is cooled, the dissolved NiO precipitates in mud-like shape as shown in Fig. 4(c). On the contrary, if NiO is dissolved in basicity way, hot corrosion is

impeded. As shown in Fig. 4(c), the mud-like NiO is easy to spall from the substrate, leading to the mass loss of samples. The as-cast Ni−12Cr−6.8Al alloy has the highest peaks of NiO (see Fig. 7). Meanwhile, the as-cast Ni−12Cr−6.8Al alloy forms Ni_3S_2 after hot corrosion, while the other two alloys do not. The two reasons mentioned above result in the mass loss of Ni−12Cr−6.8Al alloy being the highest among the as-cast samples. The interesting thing is that with the content of Cr increases, the mass loss of as-cast alloy decreases, as shown in Fig. 1.

It mainly lies in three aspects. Firstly, the sulfides of Cr are more stable than those of Ni and Al, and selective sulfidation of Cr suppresses the formation of other sulfides. The newly-generated sulfides of Cr can form spinel phase ($NiCr_2S_4$), which can effectively retard the diffusion of cations, as studied by LU et al [15]. In this investigation, the formation of sulfides of Ni and Cr can be proved by the elements map shown in Fig. 5. So, the insufficient concentration of Cr leads to the rapid formation of Ni sulfides, causing rapid corrosion. The obvious diffraction peaks of Ni_3S_2 then appear (Fig. 7) and Ni−12Cr−6.8Al alloy exhibits higher kinetics curve (Fig. 1(a)). Secondly, as pointed out by RAPP [14], the basic dissolution of chromia during the hot corrosion is dependent on the oxygen pressure. Because of the pressure of oxygen is usually higher at the interface between gas and salt than that between the oxide/salt interface, chromia is hard to experience a negative gradient of solubility, although the negative gradient exists indeed at the flaws and grain boundaries. Finally, plenty of Cr can promote the formation of protective scale as well as improve the self-healing ability of the scale.

Therefore, it can be concluded that when Cr is insufficient (as-cast Ni−12Cr−6.8Al and Ni−16Cr−6.8Al alloys), it is easier for Ni to react with sodium sulfate and produce lots of NiO, then the second type of low temperature hot corrosion takes place and the kinetics of the two alloys follows the parabolic law. On the contrary, the as-cast Ni−20Cr−6.8Al alloy with plenty of Cr and Ni is hard to react with sodium sulfate. Oxidation is the main reaction occuring on the surface and the kinetics curves really seem like to exhibit the logarithm relationship. But the initial state is different from that of the preoxidized samples, the kinetics curve of as-cast Ni−20Cr−6.8Al alloy does not follow the logarithm relationship but the power law.

4.2 LTHC mechanism of preoxidized Ni−Cr−Al based alloy

As discussed above, the hot corrosion mechanism of as-cast alloys is hardly the same with that of the preoxidized alloys. The kinetics of the preoxidized samples follows the logarithmic law which is much slower than the parabolic law due to of the existence of the preoxidation layer. This is mainly because the existence of the preoxidation layer. When the deposited fused salt contacts with the oxide layer, the dissolution of oxides begins, since the rate of dissolution is slower than the as-cast alloy, the degree of hot corrosion is in a relatively low level. At the same time, the fused salt can diffuse through the oxide layer and reach the surface of the substrate, causing the hot corrosion of the substrate. The preoxidation layer serves as a protective barrier between the circumstance and the alloy. Once the oxide layer is worn out or peels off from the alloy, the corrosion would be accelerated. Thus, the hot corrosion behavior is remarkably affected by the characteristics of the oxide layer formed during the preoxidation, such as the thickness, adhesion, amount of defects and inner force. If it is easier for the fused salt to pass through the layer, the sample is easier to be corroded.

The preoxidized Ni−16Cr−6.8Al alloy possesses both the thickest and most adhesive oxide layer (Fig. 3 and Table 2). At the same time, although the preoxidized Ni−20Cr−6.8Al alloy has thinner protective oxide layer, its mass loss is less than that of the preoxidized Ni−12Cr−6.8Al alloy. This maybe lies in the influence of Cr. The Cr content in the substrate of preoxidized Ni−20Cr−6.8Al alloy is much higher than that in the substrate of preoxidized Ni−12Cr−6.8Al alloy. Therefore, the substrate of Ni−12Cr−6.8Al alloy is easier to be corroded according to the above discussion. What is more, the outwards diffusion of cations such as Cr ions and Ni ions are delayed by the formation of spinel sulfides of Ni and Cr, as shown in Fig. 10. Thus, it is easy for the preoxidation layer of Ni−12Cr−6.8Al alloy to spall from the substrate after hot corrosion. After spalling, the actual Cr content in the substrate is even lower than that of the as-cast alloy. Since the hot corrosion of preoxidized alloys is harder than that of the as-cast alloy, the kinetics curves would all follow the logarithm law. But due to the preoxidation layer of preoxidized Ni−12Cr−6.8Al spalling during hot corrosion, the kinetics of preoxidized Ni−12Cr−6.8Al alloy is similar with that of as-cast Ni−20Cr−6.8Al alloy (Fig. 1).

5 Conclusions

1) The hot corrosion kinetics of Ni−*x*Cr−6.8Al alloys is studied. The kinetics of Ni−12Cr−6.8Al and Ni−16Cr−6.8Al based alloys fit the parabolic law well, while that for Ni−20Cr−6.8Al based alloy fits the power law. The kinetics of the preoxidized samples all obeys the logarithmic law. Both increasing the concentration of Cr and preoxidation can greatly improve the resistance to

hot corrosion of the alloy.

2) After the low temperature hot corrosion at 873 K for 100 h in the mixed sodium sulfate+sodium chloride salt, Ni−12Cr−6.8Al alloy suffers a catastrophic corrosion and the products are mainly NiO and Ni_3S_2. Ni−16Cr−6.8 Al alloy suffers a less serious corrosion and Ni−20Cr−6.8Al alloy suffers the least, and the products are NiO, NiO and Cr_2O_3, respectively. After corrosion, the products of the preoxidized alloys are all mainly oxide scales such as Al_2O_3, Cr_2O_3 and NiO but no sulfides.

3) The hot corrosion mechanism of as-cast alloy can be well explained by the acid-base melting model, but the LTHC behavior of preoxidized alloys is mainly determined by the properties of the oxide layer formed in the previous preoxidation.

References

[1] YANG Xiu-ying, PENG Xiao, WANG Fu-hui. Hot corrosion of a novel electrodeposited Ni−6Cr−7Al nanocomposite under molten $(0.9Na, 0.1K)_2SO_4$ at 900 °C [J]. Scripta Materialia, 2007, 57: 891−894.

[2] NIU Y, GESMUNDO F, VIANI F. The corrosion of Ni_3Al in a combustion gas with and without Na_2SO_4-NaCl deposits at 600−800 °C [J]. Oxidation of Metals, 1994, 42(3−4): 265−284.

[3] OU Xue-mei, SUN Zhi, SUN Min. Hot-corrosion mechanism of Ni−Cr coatings at 650 °C under different simulated corrosion conditions [J]. Journal of China University of Mining & Technology, 2008, 18(3): 444−448.

[4] GLOBEL J A, PETTIT F S. Na_2SO_4 induced accelerated oxidation (hot corrosion) of nickel [J]. Metall Trans,1970, 4: 1943−1954.

[5] BORNSTEIN N S, de CRESCENTE M A. The relationship between compounds of sodium and sulfur and sulfidation [J]. Metallurgical and Materials Transactions B, 1969, 4(8): 1799−1810.

[6] BORNSTEIN N M, de CRESCENTE M A. The role of sodium in the accelerated oxidation phenomenon termed sulfidation [J]. Metall Trans, 1971, 2(10): 2875−2883.

[7] ZHANG Zhi-liang, LI Da-yi, DONG Xue-qing. Microstructural study of Fe−Cr−Al/Al composite coatings during oxidation and sulfidation at 900 °C [J]. Acta Metallurgica Sinica, 2007, 20(2): 87−94.

[8] LANG Feng-qun, YU Zhi-ming. Corrosion behavior of Fe-40Al sheet in N_2−11.2O_2−7.5CO_2 atmospheres with various SO_2 contents at 1273 K [J]. Intermetallics, 2003, 11(2): 135−141.

[9] GOWARD G E. Microstructures and properties of thermal barrier coatings Plasma-Sprayed by nanostructured Zirconia [J]. Surface and Coatings Technology, 1998, 108−109: 73−84.

[10] STRAFFORD K N, DATTA P K, HAMPTON A F. The influence of minor additions of the reactive elements Al, Zr, Hf or Si on the corrosion of Ni-Cr alloys in an oxygen-sulphur environment at 700 °C [J] .Corrosion Science, 1989, 29(6): 673−702.

[11] RAPP R A. Hot corrosion of materials [J]. Pure & Appl Chem, 1990, 62(1): 113−122.

[12] FELIX P. Deposition and corrosion in gas turbines [M]. London: Appl Sci Pub, 1972: 331−338.

[13] LI Yun, GUO Jian-ting, YUAN Chao, YANG Hong-cai, XU Ning, SHEN Zhi-ming. Hot corrosion of nickel-base cast superalloy K35 at 800 °C [J]. Journal of Chinese Society for Corrosion and Protection, 2005, 25(4): 250−255. (in Chinese)

[14] RAPP R A. Hot corrosion of materials: A fluxing mechanism?[J]. Corrosion Science, 2002, 44(2): 209−221.

[15] LU Yun-xia, CHEN Wen-xu, EADIE R. The sulfidation/oxidation resistance of two Ni−Cr−Al−Y Alloys at 700 °C [J]. Acta Metallurgica Sinica, 2004, 17(2): 166−174.

Ni−*x*Cr−6.8Al 基合金热腐蚀行为

韩 朝[1]，刘 咏[1]，王 岩[1]，李维杰[1]，汤慧萍[2]

1. 中南大学 粉末冶金国家重点实验室，长沙 410083；
2. 西北有色金属研究院 多孔金属材料国家重点实验室，西安 710016

摘 要：研究铸态和预氧化态 Ni-*x*Cr-6.8Al 基合金在 Na_2SO_4+25%NaCl 混合盐中 873 K 时的热腐蚀行为。结果表明：Ni−*x*Cr−6.8Al 基合金的质量损失随着 Cr 元素含量的增加而减少，预氧化可以明显改善材料的抗热腐蚀性能，并且与 Cr 含量无关。Ni−12Cr−6.8Al 基和 Ni−16Cr−6.8Al 基合金的热腐蚀动力学遵循抛物线规律，Ni−20Cr−6.8Al 基合金遵循指数规律，所有的预氧化试样的热腐蚀动力学都符合对数规律。铸态合金热腐蚀的机理可以用酸碱熔融模型解释，而预氧化合金的热腐蚀机理在很大程度上由预氧化过程中形成的氧化层的性质决定。

关键词：Ni-Cr-Al 基合金；热腐蚀；Cr 含量；预氧化；动力学；腐蚀机理

(Edited by FANG Jing-hua)